Linearity of volume hologram out-coupling for wavelength-division demultiplexing

X. Deng, F. Zhao, Zhenhai Fu, Jizuo Zou, Jie Qiao, G. Kim, Ray T. Chen

Microelectronics Research Center, Department of Electrical and Computer Engineering,
The University of Texas, Austin, Texas 78758,U.S.A.

ABSTRACT

Close-form expressions are used to analyze the spatial and angular linearity of the out-coupling volume holograms in wavelength division multiplexing/demultiplexing (WDM/WDDM). Optimal spatial linear out-coupling regimes are located. Some design criteria for volume holographic WDDM applicable to $800nm$, $1300nm$, and $1550nm$ optical wavelength window are addressed. As a design example, we deploy these criteria to design a passive surface normal input/output wavelength division demultiplexer (DMUX) working in the wavelength range of $768 \sim 864nm$. Coupling of the demultiplexed optical signal from the substrate modes to a linear multi-mode fiber array is verified with experiment. The importance of the spatial linearity of the out-coupling in volume holographic WDDM structure is highlighted and possible coupling of the signal to linear single-mode fiber array is mentioned.

Keywords: Linearity of out-coupling, Normalized dispersion abilities, Normalized wavelength/frequency nonlinearities, Design tradeoffs, Volume holographic gratings, Wavelength-division multiplexing, Fiber optics and optical communications

1. INTRODUCTION

Wavelength-division multiplexing (WDM) has becoming the major candidate for the next generation telecommunication network despite of several other competing yet possible coexisting technologies.[1–4] Terabit per second transmission experiments has also been demonstrated with data networks by using WDM.[5] WDM has several advantages. It can efficiently exploit the huge bandwidth of single mode fibers. WDM is also promising on constructing different levels of transparency to optical transmissions (*e.g.*, independent of data bit-rate, modulation format, or protocol), allowing nice upgrading and backward compatibility of the current network, which makes WDM the key to tomorrow's developments on data, voice, imaging, and video communications.[6–9] Passive optical networks (PON) and corresponding passive devices must be developed to meet the requirements to maximize the market volume and minimize the amortized equipment costs in near future.

The challenges are put back to wavelength demultiplexing when the wavelength separation among channels becoming smaller and the number of channel count increases. A channel separation about $0.8nm$ around $1550nm$ wavelength or smaller, and a number of channel count bigger than 16, is desired for telecommunications. More cost sensitive communications under shorter distances like the local area networks (LAN's) and metropolitan area networks (MAN's and WAN's) have different requirements. Bigger channel spacing and a channel-number count of $4 \sim 16$ is expected.

Volume holographic multiplexers/demultiplexers (H-MUX's/H-DMUX's) have very simple structures and are more cost-effectiveness over the other scenarios such as arrayed-waveguide gratings (AWG's)[10,11] and micro-optics.[12] Very flexible channel spacing, *e.g.*, from $2.0nm$ to $30nm$, were demonstrated with passive H-MUX's/H-DMUX's.[13–15] H-MUX's/H-DMUX's may be used to guide, deflect, tap, broadcast, route, interchange, interconnect, multiplex or demultiplex multi-wavelength optical signals.[14–22] Recent study indicates that the grating based MUX/DMUX with proper selection of device material and optimal structure can operate with no active temperature control.[23] However, the out-coupling of these H-NUX's/H-DMUX 's is inherently nonlinear. Cautious design must be exercised especially when the count of channels increases and channel spacing decreases as in dense-WDM/WDDM applications.

Send correspondence to Dr. Chen (E-mail: raychen@uts.cc.utexas.edu)

In this paper, we focus on the nonlinearity of the out-coupling in H-MUX's/H-DMUX's. In Section 2, the dispersion abilities of these grating-based demultiplexers are reviewed. Asymmetric properties between the input and output coupling of optical signals by volume holograms are discussed. Close-form expressions are used to analyze the spatial and angular linearity of the out-coupling volume holograms in Section 3. Some design criteria for H-MUX's/H-DMUX's such as the dispersion abilities and power losses are addressed. Design trade-offs are emphasized. In Section 5, we deploy these criteria to design and package a passive surface normal input/output H-DMUX working in the wavelength range of $768 \sim 864nm$.

2. DISPERSION ABILITIES OF A PASSIVE HOLOGRAPHIC MULTIPLEXER/DEMULTIPLEXER

Dispersion abilities, among the key parameters of a multiplexer or demultiplexer that are independent of the multiplexing/demultiplexing structure,[24] are the most important intrinsic characteristics besides the passing bandwidth and insertion loss of a device. It by and large determines the performance of a device.

The working principle of a holographic multiplexer is the same as that of a holographic demultiplexer. Besides, the real challenges come from demultiplexing for a WDM system compared with multiplexing. Hence, only the properties of demultiplexing structures will be addressed. In a much general sense, the central part of the H-DMUX consists of a piece of volume holographic grating. Its spatial position in reference to the incoming and out-going signals is schematically illustrated in **Figure 1**.

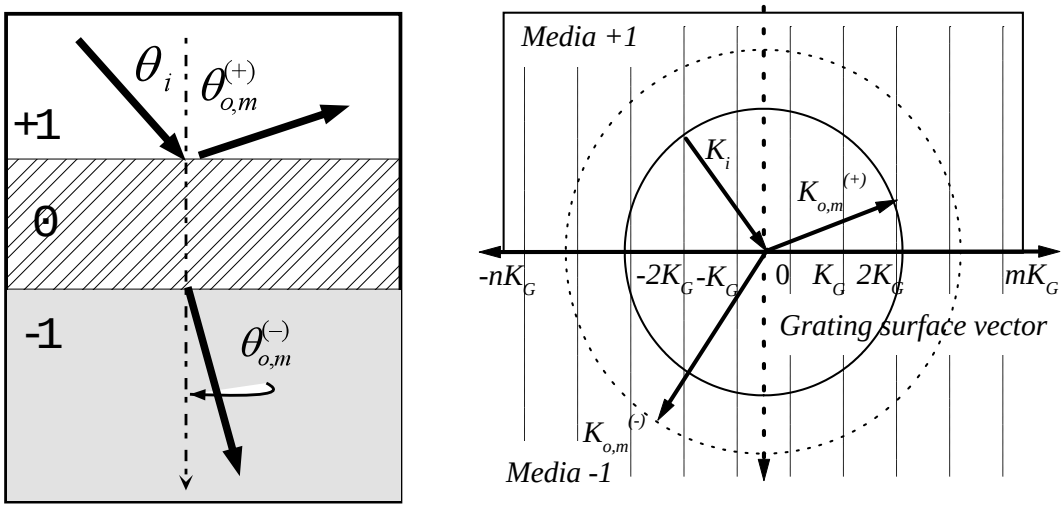

Figure 1. Diffraction geometry of holographic gratings. The space is divided into three layers, namely, the incident space (or *superstrate*), the grating layer, and the transmission layer (or *substrate*), denoted with +1, 0, -1, respectivly. The phase matching condition is illustrated at the right side with the wave vectors and the grating vector, $K_G \equiv K$. $K = 2\pi/\Lambda_x$, and Λ_x is the lateral period of the grating.

The dispersion can be treated very accurately as a diffraction process. In **Figure 1**, the media are divided into three layers, namely, *superstrate, grating,* and *substrate*, which are labeled as $+1, 0$, and -1 region, respectively.[25] Symbols of their electrical permittivity carry the same superscripts. The thickness of the grating is t. Collimated quasi-plane optical waves are incident from an angle θ_i through the superstrate towards the grating layer. From rigorous coupled wave theory (RCWT),[25–28] the angular direction of the $m-th$ order harmonics of the reflecting (*superscript:*+) or transmitting diffracted wave (*superscript:*-) is $\theta^{(\pm)}_{o,m}$. *The normalized total dispersion ability (NTDA)* of the grating,[23] $D^{(\pm)}_t(\lambda) \equiv \lambda \frac{d\theta^{(\pm)}_{o,m}}{d\lambda}$, is

$$D_t^{(\pm)}(\lambda) = \tan(\theta_{o,m}^{(\pm)}) \cdot [D_M^{(+)}(\lambda) - D_M^{(\pm)}(\lambda)] + D_G^{(\pm)}(\lambda) \cdot (1 - D_M^{(+)}(\lambda)), \tag{1}$$

$$D_M^{(\pm)}(\lambda) \equiv \frac{\lambda}{n^{(\pm)}(\lambda)} \cdot \frac{dn^{(\pm)}(\lambda)}{d\lambda}, \quad n_r^{(\pm)}(\lambda) \equiv \frac{n^{(+)}(\lambda)}{n^{(\pm)}(\lambda)} \tag{2}$$

$$D_G^{(\pm)}(\lambda) \equiv \frac{\sin(\theta_{o,m}^{(\pm 1)}) - n_r^{(\pm)}(\lambda)\sin(\theta_i)}{\cos(\theta_{o,m}^{(\pm)})}. \tag{3}$$

λ is the wavelength in vacuum. For dielectric media,their permeability μ can be regarded as that of vacuum, and $\sqrt{\varepsilon^{(\pm)}\mu} = n^{(\pm)}(\lambda)$ is the refractive index of the material. $n_r^{(\pm)}(\lambda)$ is the relative refractive indices. $D_M^{(\pm)}(\lambda)$ and $D_G^{(\pm)}(\lambda)$ represents the *normalized material dispersion ability (NMDA)* and the *normalized geometrical dispersion ability (NGDA)*, respectively. When the superstrate and the substrate is made of the same material, Eq.(1) becomes

$$D_t^{(\pm)}(\lambda) = D_G^{(\pm)}(\lambda) \cdot (1 - D_M^{(+)}(\lambda)). \tag{4}$$

Another useful quantity is the *NTDA* expressed in frequency instead of wavelength, $D_{t,\nu}^{(\pm)}(\nu) = \nu \frac{d\theta_{o,m}^{(\pm)}}{d\nu}$, ν is the optical frequency of the signal. It is straight forward to show that

$$D_{t,\nu}^{(\pm)}(\nu) = -D_t^{(\pm)}(\lambda). \tag{5}$$

Therefore, Eqs.(1)-(4) are applicable to discussions with frequencies as well as wavelengths. A set of curves of the *NTDA* for $n_r^{(\pm)} = 1$ is plotted in **Figure 2**.

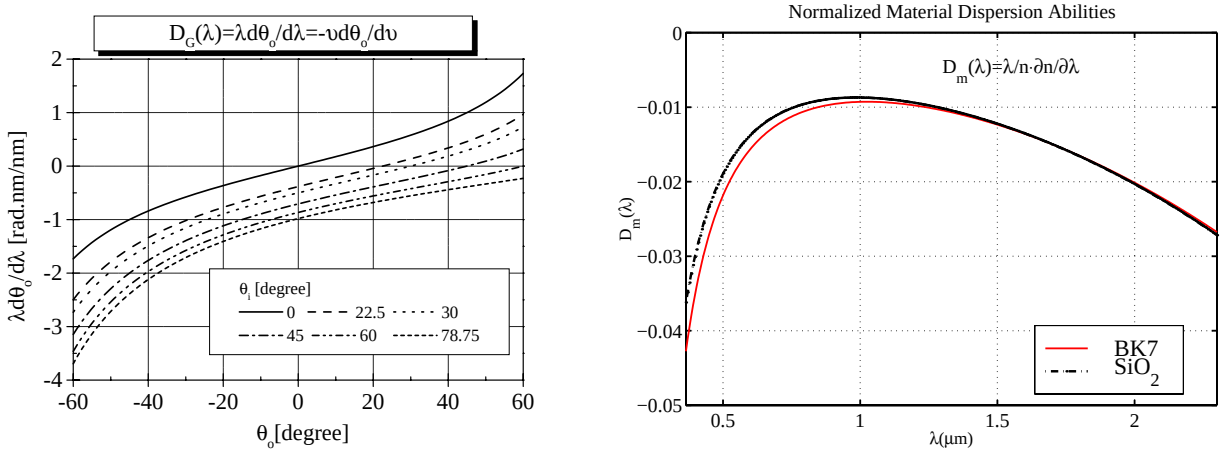

Figure 2. *Left:* Normalized total dispersion abilities of gratings, assuming $n_r^{(\pm)} = 1$. *Right:* Normalized material dispersion abilities of BK7 glass and synthetic fused silica.

Eq.(3) has been used as the *NTDA* for WDM/WDDM applications in many literatures,[14–17,29] which introduces an error around $-D_M^{(+)}(\lambda)$ that is important for dense wavelength-division-multiplexing/demultiplexing (D-WDM/D-WDDM) applications. For most of the optical media, the *NMDA* is a slow varying function of wavelength and is usually very small. For example, the *NMDAs* of BK7 glass and synthetic fused silica (SiO_2) plotted in **Figure 2** are around $-0.006 \sim -0.02$ in the wavelength range of $0.5\mu m \leq \lambda \leq 2.3\mu m$. Therefore, even for the wide wavelength-division-multiplexing/demultiplexing (W-WDM/W-WDDM) having been proposed, variations of

the wavelengths are no more than $100nm$, the dispersion correction coming from the material dispersions as in Eq.(1) could be regarded as constants,*i.e.*, $D_M^{(\pm)}(\lambda) \approx D_M^{(\pm)}(\lambda_c)$, while λ_c is the central wavelength of the device. Hence, the major contribution to the dispersion abilities comes from the grating structural dispersion that is two orders of magnitude bigger than that of most of the material dispersion.

The asymmetric property of θ_i and $\theta_{o,m}^{(\pm)}$ in Eq. (3) may strongly alter the performance of a H-MUX/H-DMUX. A passive H-MUX/H-DMUX must have a big enough yet proper value of the *NTDA* to separate incoming multi-wavelength signal, and route the signals to different physical out-going points,which is addressed below.

3. LINEARITY OF DEMULTIPLEXING BY A VOLUME HOLOGRAM

Dispersed by the grating, optical signals of different wavelengths will be routed to individual output ports — usually optical fibers — in a typical H-DMUX. A simple way to do this discrimination of different wavelengths involves focusing the diffracted beams to a linearly spaced fibers permanently fixed in a V-groove, as shown in **Figure 3**. One of the advantages of such an arrangement is that one eliminates necessary multiple alignments for individual fiber by simultaneously coupling all the channels out, hence improves the throughput. However, this imposes additional constraints on the MUX/DMUX structures. Trade-offs between good linearities of the out-coupling and high dispersion abilities, compromises among the dispersion abilities and the bandwidths of the hologram, and contentions between insertion loss and polarization dependence.[23,24]

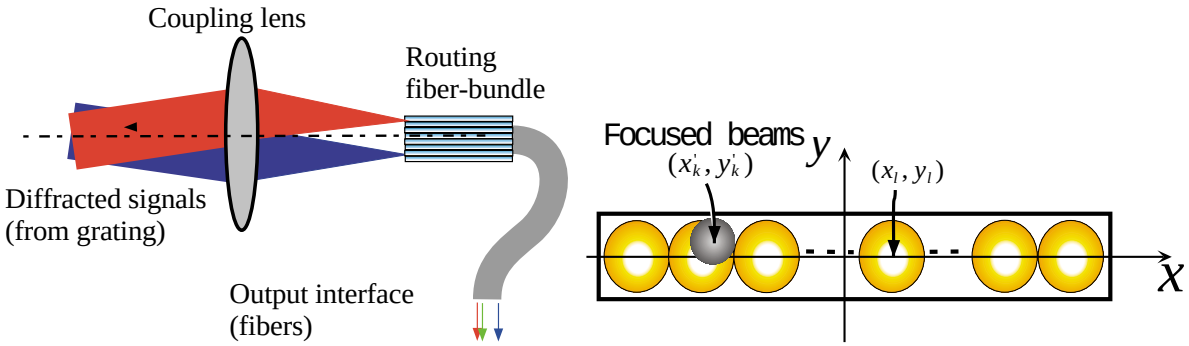

Figure 3. Coupling focused beams from free space to V-grooved linear fiber array. The fibers are centered at (x_l, y_l) while the beams are focused at (x_k', y_k'), $k, l = 1, 2, 3, ..., N_c$.

3.1. Spatial and angular nonlinearities of the out-coupling to fiber array

Given a N_c-channel WDM/WDDM system, its working wavelengths usually locate on a linear-spaced frequency grid such as those recommended by the International Telecommunication Union (*ITU*) standards in telecommunications. For simplicity, we symbolically write the wavelengths as $\lambda_l, \lambda_l \nu_l \equiv c, l = 1, 2, 3, ..., N_c$. Let the foci of the lens be f , the out-going beams of wavelength λ_l is focused at (x_l, y_l) that should locate near $(x_l^{(i)}, y_l^{(i)})$,the center of the $l-th$ fiber. The spacing between adjacent fiber centers is denoted by s_0. The *spatial nonlinearity of the out-coupling (SNOC)* can be measured with the following standard deviations of the focused spots

$$\sigma_S = \left[\frac{1}{N_c} \sum_{l=1}^{N_c} \frac{(x_l - x_l^{(i)})^2 + (y_l - y_l^{(i)})^2}{s_0^2} \right]^{\frac{1}{2}} . \tag{6}$$

Were $(\theta_{l,x}, \theta_{l,y})$ the angular direction of the $l-th$ beam relative to the primary optical axis of the focusing lens, and $(\theta_{l,x}^{(i)}, \theta_{l,y}^{(i)}) \equiv (\tan^{-1}(x_l^{(i)}/f), \tan^{-1}(y_l^{(i)}/f))$ is the corresponding angular position of the fiber center, the *SNOC* is

$$\sigma_S = \frac{f}{s_0}\left[\frac{1}{N_c}\sum_{l=1}^{N_c}\left(\tan(\theta_{l,x}) - \tan(\theta_{l,x}^{(i)})\right)^2 + \left(\tan(\theta_{l,y}) - \tan(\theta_{l,y}^{(i)})\right)^2\right]^{\frac{1}{2}}. \tag{7}$$

The H-MUX/H-DMUX usually works under the condition that $\theta_{l,y} = 0$ while an ideal linear fiber array implies $\theta_{l,y}^{(i)} = 0$. Hence, for small angles, $\tan\theta \approx \theta, \overline{\delta\theta} \approx \frac{s_0}{f}$, Eq. (7) can be approximated as

$$\sigma_S \approx \sigma_A = \left[\frac{1}{N_c}\sum_{l=1}^{N_c}\left(\frac{\theta_{l,x} - \theta_{l,x}^{(i)}}{\overline{\delta\theta}}\right)^2\right]^{\frac{1}{2}} \tag{8}$$

in which the average angular spacing is

$$\overline{\delta\theta} = \frac{1}{N_c - 1}\sum_{l=1}^{N_c-1}\left|\theta_{l+1,x}^{(i)} - \theta_{l,x}^{(i)}\right| = \frac{\theta_{N_c,x}^{(i)} - \theta_{1,x}^{(i)}}{N_c - 1}. \tag{9}$$

The advantage of using σ_A is that we don't need to care about the concrete focusing lens and the exact spacing of the linear fiber array, while σ_S is more accurate on reflecting the actual coupling misalignment.

3.2. Linearity of volume hologram dispersion abilities

The *SNOC* is mainly determined by the dispersion relation*. Let $(\theta_{l,x}^{(i)}, \theta_{l,y}^{(i)}) = (\theta_{o,m}^{(\pm)} - \theta_{c,x}^{(\pm)}, \theta_{c,y}^{(\pm)})$, $\theta_{c,x}^{(\pm)}$ and $\theta_{c,y}^{(\pm)}$ are constants, without loosing generality. One readily obtains

$$\frac{dx_l}{d\lambda} = \frac{d[f\tan(\theta_{l,x}^{(i)})]}{d\lambda} = \frac{f}{\lambda\cos^2(\theta_{l,x}^{(i)})}\cdot D_t^{(\pm)}(\lambda) \tag{10}$$

and

$$\frac{d^2x_l}{d\lambda^2} = \frac{f}{[\lambda\cos(\theta_{l,x}^{(i)})]^2}\cdot\left\{2D_t^{(\pm)}(\lambda)^2\tan(\theta_{l,x}^{(i)}) + \lambda^2\frac{d^2\theta_{o,m}^{(\pm)}}{d\lambda^2}\right\}. \tag{11}$$

Similarly, the corresponding quantities for channels locating on frequency grid are

$$\frac{dx_l}{d\nu} = \frac{f}{\nu\cos^2(\theta_{l,x}^{(i)})}\cdot D_{t,\nu}^{(\pm)}(\nu), \tag{12}$$

$$\frac{d^2x_l}{d\nu^2} = \frac{f}{[\nu\cos(\theta_{l,x}^{(i)})]^2}\cdot\left\{2D_{t,\nu}^{(\pm)}(\nu)^2\tan(\theta_{l,x}^{(i)}) + \nu^2\frac{d^2\theta_{o,m}^{(\pm)}}{d\nu^2}\right\}. \tag{13}$$

Using Eq. (5) and $\lambda\frac{d}{d\lambda}\left(\lambda\frac{d\theta_{o,m}^{(\pm)}}{d\lambda}\right) = \nu\frac{d}{d\nu}\left(\nu\frac{d\theta_{o,m}^{(\pm)}}{d\nu}\right)$, we find

$$\nu^2\frac{d^2\theta_{o,m}^{(\pm)}}{d\nu^2} = \lambda^2\frac{d^2\theta_{o,m}^{(\pm)}}{d\lambda^2} + 2\lambda\frac{d\theta_{o,m}^{(\pm)}}{d\lambda} = \lambda^2\frac{d^2\theta_{o,m}^{(\pm)}}{d\lambda^2} + 2D_t^{(\pm)}, \tag{14}$$

and

*Sometimes one may choose a configuration like working off-axis to optimize the coupling linearity. However, an off-axis structure may introduce aberrations that reduce the coupling efficiency and increase the crosstalk among neighbor fibers. A much more straight forward method to evaluated the nonlinearity is to check the *NTDA*.

$$\lambda^2 \frac{d^2\theta_{o,m}^{(\pm)}}{d\lambda^2} = \left\{ \frac{D_M^{(+)} - D_M^{(\pm)}}{\cos^2(\theta_{o,m}^{(\pm)})} + [1 - D_M^{(+)}] \cdot [1 + D_G^{(\pm)} \cdot \tan(\theta_{o,m}^{(\pm)})] - 1 \right\} D_t^{(\pm)} \tag{15}$$

by ignoring all the higher order derivatives related to the material dispersion. For simplicity, we assume $n_r^{(\pm)} = 1$ from now on. Hence, Eqs.(14)-(15) become

$$\nu^2 \frac{d^2\theta_{o,m}^{(\pm)}}{d\nu^2} = D_G^{(\pm)}(\lambda)^2 \tan(\theta_{o,m}^{(\pm)}) + 2D_t^{(\pm)}(\lambda) \tag{16}$$

and

$$\lambda^2 \frac{d^2\theta_{o,m}^{(\pm)}}{d\lambda^2} = D_G^{(\pm)}(\lambda) \cdot D_t^{(\pm)}(\lambda) \cdot \tan(\theta_{o,m}^{(\pm)}) = D_G^{(\pm)}(\lambda)^2 \tan(\theta_{o,m}^{(\pm)}). \tag{17}$$

The term $\nu^2 \frac{d^2\theta_{o,m}^{(\pm)}}{d\nu^2}$ dominates the quantity in parenthesis in Eq.(13) as $\lambda^2 \frac{d^2\theta_{o,m}^{(\pm)}}{d\lambda^2}$ does in Eq.(11) unless $|\theta_{o,m}^{(\pm)}| \sim |\theta_{l,x}^{(i)}| \ll 1$. The nonlinearity of the out-coupling is mainly determined by that of the hologram dispersion ability. Eq.(17) is zero when $\theta_{o,m}^{(\pm)} = 0$, which is the best angular linearity for equal-wavelength-spacing demultiplexing. This states that the smaller the output angle the better the output linearity in general. For littrow mounts, $\theta_{o,m}^{(\pm)} \approx -\theta_i$, $\lambda^2 \frac{d^2\theta_{o,m}^{(\pm)}}{d\lambda^2} \approx -4\tan^3(\theta_i)$, the nonlinear behavior of the output manifests very quickly with increasing littrow angle. The conclusion holds for equal-frequency-grid demultiplexing as well. As plotted in Figure 4, the smaller the value of $\lambda^2 \frac{d^2\theta_{o,m}^{(\pm)}}{d\lambda^2}$ or $\nu^2 \frac{d^2\theta_{o,m}^{(\pm)}}{d\nu^2}$, the better the linearity of the out-coupling from the hologram. The amplitude of $\nu^2 \frac{d^2\theta_{o,m}^{(\pm)}}{d\nu^2}$ in general is bigger than that of $\lambda^2 \frac{d^2\theta_{o,m}^{(\pm)}}{d\lambda^2}$.Thus, one has stronger nonlinearity when using equal-frequency-grid channels (as proposed by ITU-T) if using single grating-based demultiplexing technique.

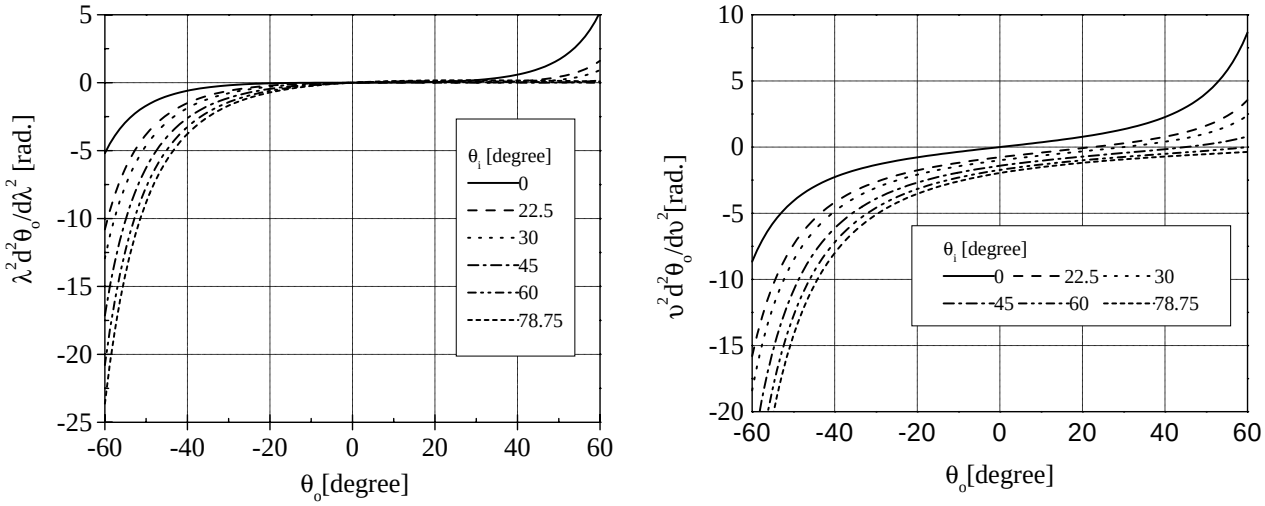

Figure 4. The normalized nonlinearity $\nu^2 \frac{d^2\theta_{o,m}^{(\pm)}}{d\nu^2}$ and $\lambda^2 \frac{d^2\theta_{o,m}^{(\pm)}}{d\lambda^2}$ for different $(\theta_i, \theta_{o,m}^{(\pm)})$ diffraction geometries.

For out-coupling with a linear fiber array, trade-offs have to be made between good linearities of the out-coupling and high dispersion abilities, as well as compromises among the dispersion abilities and the bandwidths of the hologram, and contentions between insertion loss and polarization dependence.[24]

4. OUT-COUPLING OF A HOLOGRAPHIC WAVELENGTH-DIVISION DEMULTIPLEXER

Under certain circumstances, especially for heterogenous input/output interfaces as developed for one-way communications,[30] the out-coupling may tolerate much stronger nonlinearity depending on the filtering characteristics of the multiplexer/demultiplexer. The insertion loss spectrum provides almost complete information of the device.

The insertion loss comes from two major sources,namely, the holographic grating and the out-coupling interfaces that usually involves fibers. Holograms or gratings of high diffraction efficiency and good wavefront quality are commercially available.[32] Thus, the bottle-neck of design usually is the out-coupling interface that dominates the total loss of the device. Suppose no numerical aperture (NA) mismatch, *i.e.*, the NA of the beam should be no bigger than that of the fiber in V-groove, we can use the *"energy-in-bucket (EIB)"* model to characterize the coupling from free space to fibers.[23,24] Suppose the transmission function of the fiber centering at (x_l, y_l) is $W_{F,l}(x, y)$, and the intensity distribution of the focused beam on the fiber facet is $I_k(x, y)$, then the normalized energy in the fiber (as a "*bucket*" collecting light) is

$$E_{k,l} = \frac{\int\int_{-\infty}^{+\infty} W_{F,l}(x,y) I_k(x,y) dxdy}{\int\int_{-\infty}^{+\infty} I_k(x,y) dxdy}, \quad k, l = 1, 2, 3, ...N_c. \tag{18}$$

Similarly, the cross-talk from channel k to channel l can be defined as

$$R_{k,l} = -10 \log_{10} \left(\frac{E_{k,l}}{E_{l,l}} \right) \quad (dB). \tag{19}$$

For Gaussian beams with a beam width of 2σ and step-index out-coupling fibers, a set of curves obtained by using Eq.(18) for different coupling conditions of the normalized beam width, σ/R_f, and the normalized misalignment distance, x/R_f, as R_f is the fiber radius, are presented in **Figure 5.** According to **Figure 5**, devices with heterogenous interfaces such as those using a smaller core-size ratio for input fiber than the outputs[30] are more robust. It buys one a very small insertion loss ($1.0 \sim 1.5dB$) and a wide passing band for each channel, which in turn can tolerate more severe dispersion nonlinearity. However, MUX's/DMUX's with homogeneous interfaces have much wider applications in current network. The spatial linearity of the out-coupling becomes more important when considering linear single-mode fiber arrays.[23] The input and output fibers as the demultiplexing interfaces are assumed the same in the following discussions.

Figure 5 can also be used to look up the cross-talk and bandwidth of individual channel. Two sets of universal curves for the maximum coupling efficiency and the normalized bandwidth $BW_n \equiv BW \cdot \frac{s_0}{\lambda_s R_f} = \frac{\Delta\lambda}{\lambda_s} \cdot \frac{s_0}{R_f}$ are shown in **Figure 6**. These figures clearly indicate the importance of controlling the size of out-coupling beams. Volume holographic gratings are phase-sensitive elements in nature. Any distortion, such as the aberration from the focusing system, inhomogeneous material distribution inside the grating, dust, *etc.*, along the propagation of the incident beam degrades the wave-front and the beam quality.[31] However, holographic or the other types of gratings with surface quality of sub-wavelength flatness across several inches are commercially available.[32]

5. A SURFACE NORMAL INPUT/OUTPUT HOLOGRAPHIC DEMULTIPLEXER

Many substrate-mode structures using holograms have been proposed and tested for optical interconnects, some are also suitable for WDM/WDDM.[24] As an example, we provide some preliminary experiment results on a surface normal wide-band H-DMUX. The design principle is applicable to dense-WDM/WDDM H-MUX's/H-DMUX's working in either $800nm$, $1300nm$, or $1550nm$ optical wavelength window as well.

The demultiplexing principle is schematically shown in **Figures 7**. The surface-normal out-coupling geometry not only simplifies the alignment but also exhibits the best linearity of out-coupling among all possible single-hologram DMUX's, as discussed in Sect. 3. The substrate with a bevel angle $\theta_B = 31.25^0$ is used to provide necessary dispersion geometry. The center wavelength of this H-DMUX is set at $\lambda_c = 812nm$. The grating is

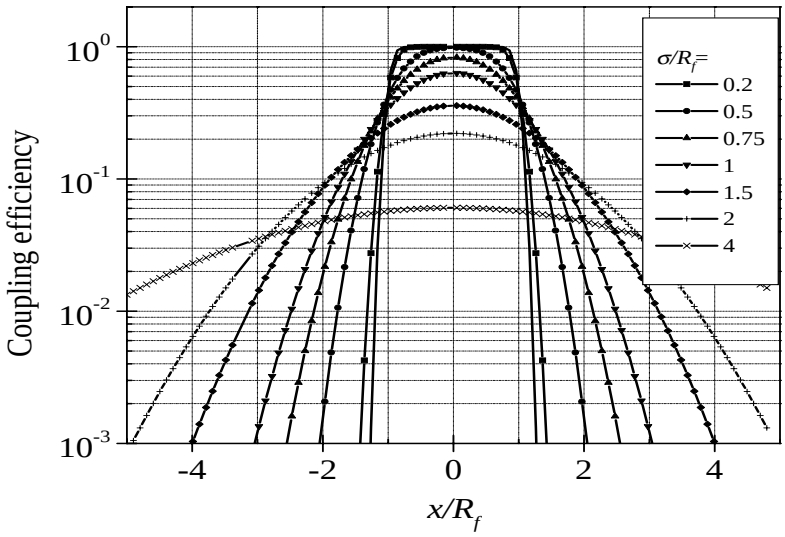

Figure 5. Energy-in-the-bucket model of coupling Gaussian beam from free space to fibers. The y-axis is the fractional energy in the fiber core while the size of the focused beam is 2σ, the misalignment between the focus center to the fiber center is x, and the fiber radius is R_f.

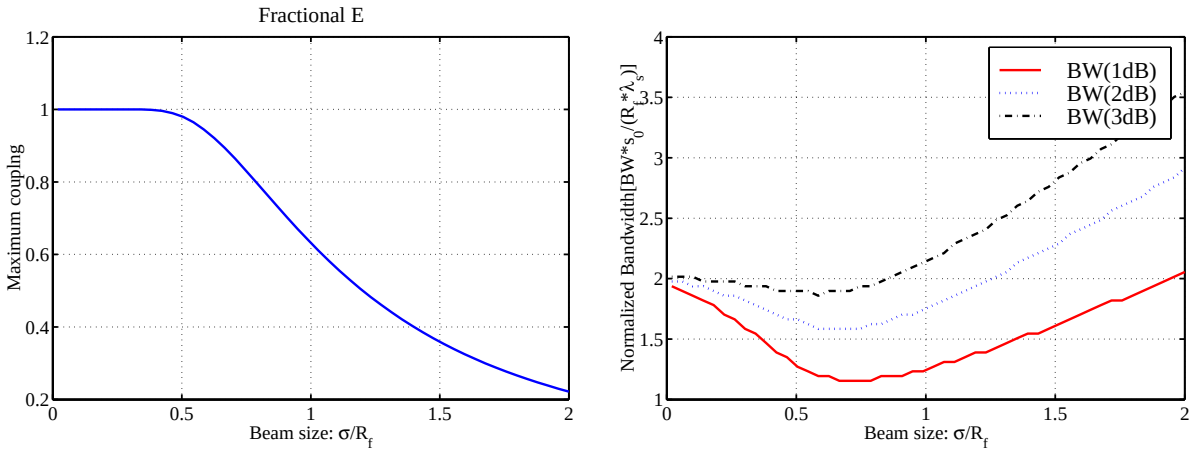

Figure 6. The maximum coupling efficiency and the passing bandwidth of a single channel extracted from the "energy-in-the-bucket (EIB)" model when coupling light from free space to fibers."BW(1dB)", "BW(2dB)", and "BW(3dB)" denotes the 1dB, 2dB and 3dB passing bandwidth, respectively, when $s_0/R_f = 4.0$. The size of the focused beam is 2σ. Misalignments between the focus center and the fiber center are neglected, $x = 0$, and the radius of the fiber is R_f.

made out of the $20\mu m$-thick DuPont holographic film HRF600-X001-20.[33–35] † A caution one must follow is the shrinkage effect due to the polymerization process in this film.[36] To precisely get the surface-normal out-coupling, pre-correction can be made to compensate the reduction of the film.[36–38]

†The choice of this material is mainly due to its easiness of the dry processing, high resolution, high sensitivity, long shelf life, and low cost,[33–35] which features almost real-time proto-typing.

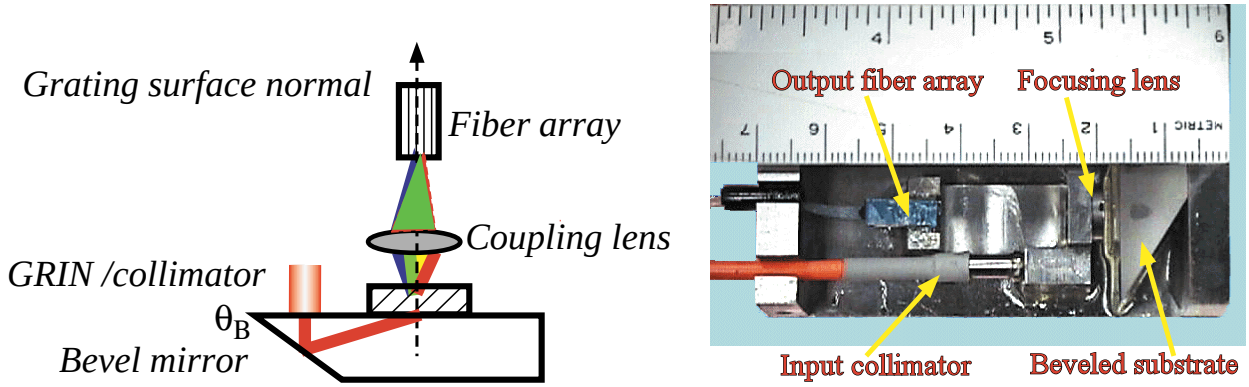

Figure 7. A surface normal input/output substrate-mode H-DMUX. The beveled substrate provides a high-index media from which the incident beam may be lauched at any angle. Geometry of high dispersion abilities are easily attainable, as well as the best out-coupling linearity. *Left:* Demultiplexing principle. *Right:* The packaged device.

The dispersion ability of the proposed structure is verified, as plotted in **Figure 8**. The slope of the measured curve is bigger than the prediction from Eq.(3), denoted as *"Experiment"* and "$d\theta/d\lambda$", respectively. The measurement are correlated as close as 99.94% with the least-square linear fitting, marked as *"Linear Fit"* in the figure. Taking $D_M(\lambda_c) \approx -0.01$ for the BK7 substrate, the mean-square-error (MSE) between the experiment curve (labeled *"Analy. Map"*) and the one predicted via Eq. (1) is only 0.4% in the wavelength range $760 \sim 830nm$. Further experiments with 24 channels at $4nm$ spacing show similar linearity in the wavelength range $760 \sim 864nm$, Ref. **Figure 8**.

Due to the limited number of fibers in the V-groove, one input and eight output channels, both interfacing $50\mu m$-core size GRIN multimode fibers, are packaged in a H-DMUX, as shown in **Figure 7**. The minimum distance between two output fibers located in the V-groove is $250\mu m$. Eight nominal center wavelengths spacing at $8.0nm$ can be chosen in the range of $760 \sim 864nm$.

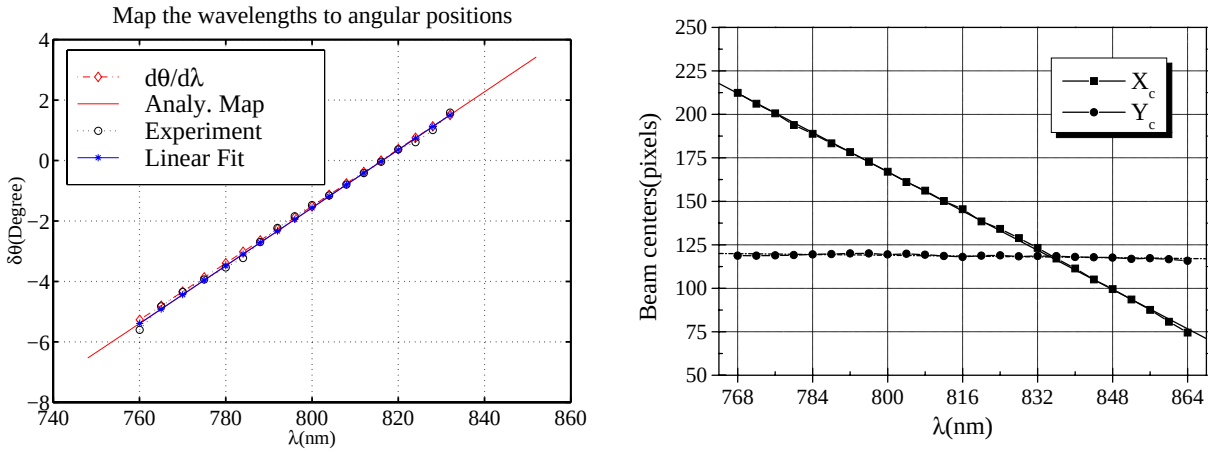

Figure 8. Measured total dispersion of the surface normal H-DMUX ("Experiment"), the theoretical prediction by using Eq.(3) ("$d\theta/d\lambda$"), the least-square linear fitted curve ("Linear Fit"), and the correct theoretical curve (overlapping with "Analy. Map") are plotted together for comparisons.

6. SUMMARIES

In this paper, the spatial and angular linearity of the out-coupling volume holograms in WDM/WDDM are analyzed with close-form expressions. Optimal spatial linear out-coupling regimes are located. Some design criteria for volume holographic WDDM applicable to $800nm$, $1300nm$, and $1550nm$ optical wavelength window, are addressed. Several universal curves, such as the maximum coupling relative to the beam size, mis-alignment, and passing bandwidth, are extracted for either homogeneous or heterogeneous I/O interfaces, which can be used to minimize power dissipation and maximize loss balance among all the channels.

As an example, we deploy these criteria to design a surface normal input/output H-DMUX. Coupling of the demultiplexed optical signal from the substrate modes to a linear multi-mode fiber array is verified with experiment. Experiments deviate from the theoretical prediction by only a MSE value of 0.4%.

Most of the formula are applicable to both holographic wide- and dense-WDM/WDDM devices, regardless the output coupling ports are multimode or single-mode fibers. This work can be extended to Bragg-grating-based structures.

Acknowledgments

We appreciate Dr. Y. Qiu for exchanging some helpful literature and Dr. J. Liu for discussions on rigorous coupled wave theories. Thanks also go to the members of the Optical Interconnect Group at Microelectronics Research Center for frequent discussions. This research is supported by Ballistic Missile Defense Organization (BMDO), Army SSDC, the Center of Optoelectronics Science and Technology (COST), the Defense Advanced Research Program Agency (DARPA), Office of Naval Research, AFOSR, DuPont Inc., Lightpath Inc., 3M Foundation, RRI, and the Advanced Technology Program (ATP) of the State of Texas.

REFERENCES

1. A.E. Willner, "Mining the optical bandwidth for a terabit per second", *IEEE Spectrum*, 34(4),32-41,(1997)
2. M. Saruwatari, "High-speed optical signal processing for communication systems", *IEICE Transactions on Communications*, E78-B(5),635-643,(1995)
3. N.S. Bergano, C.R. Davidson, "Wavelength division multiplexing in long-haul transmission systems", *J. Lightwave Technology*, 14(6),1299-1308,(1996)
4. H.A. Haus, "Molding light into solitons", *IEEE Spectrum*, 30(3),48-53,(1993)
5. R.E. Wagner, R.C. Alfferness, A.A.M. Saleh, M.S. Goodman, "MONET: Multiwavelength optical networking", *J. Lightwave Technology*, 14(6),1349-1355,(1996)
6. P. Green, "Optical networking has arrived", *IEEE Communication Magazine*, p.38,February,1998
7. J.P. Ryan, "WDM: north American deployment trends", *IEEE Communication Magazine*, p.p.40-44,February,1998
8. C. DeCusatis,"Optical data communication: fundamentals and future directions", *Optical Engineering*, 37(12) ,3082-3099,(1998)
9. R.K. Butler, D.R. Polson, "Wave-division multiplexing in the Sprint long distance network", *IEEE Communication Magazine*, p.p.52-55,February,1998
10. E. Pawlowski, M. Ferstl, H. Hellmich, B. Kuhlow, C. Warmuth, J.R. Salgueiro, "Fabrication of a multichannel wavelength-division multiplexing-passive optical net demultiplexer with arrayed-waveguide gratings and diffractive optical elements", *Applied Optics*, 38(14) ,3039-3045,(1999)
11. H.Takahashi, S. Suzuki, K. Kato, I. Nishi, "Arrayed-waveguide grating for wavelength division multi-/demultiplexer with nanometer resolution", *Electrn., Lett.*, 26, 87-88, (1990)
12. D. Intani, T. Baba, and K. Iga, "Simple optical wavelength- division multiplexer component that uses the lateral focusing scheme of a planar microlens", *Applied Optics*, 33(16), 3405- 3408,(1994)
13. C.C. Zhou, S. Sutton, R.T. Chen, B.V. Hunter, P. Dempewolf,"Four channel multimode wavelength division, multiplexer and demultiplexer based on photopolymer volume holographic gratings and substrate-guided waves", *SPIE*, Vol. 3234,136-139,(1997)

14. J. Liu, R. Chen,"Path-reversed substrate-guided-wave optical interconnects for wavelength division demultiplexing", *Applied Optics*, 38(14) ,3046-3052,(1999)
15. R. Chen, J. Liu, X. Deng, "Multimode-fiber-compatible WDM/WDDM with an ultra-large wavelength range", *SPIE*, CR71,50-71(1999) (Bellingham, Washington, USA)
16. Y.T. Huang, D. C. Su, and Y.K. Tsai, "Wavelength- division-multiplexing and demultiplexing by using a substrate-mode grating pairs", *Optics Letters*, 17(22), 1629-1631,(1992)
17. J. Chang, D. Su, Y. Huang,"Substrate-mode holographic polarization-division multi-demultiplexer for optical communications", *Applied Optics*, 33(35) ,8143-8145,(1994)
18. M.R. Wang, G.J. Sonek, R.T. Chen, T. Jannson,"Large fanout optical interconnects using thick holographic gratings and substrate wave propagation", *Applied Optics*, 31(2), 236-249,(1992)
19. R.T. Chen, H. Lu, D. Robinson, M. Wang, G. Savant, T. Jannson, "Guided-wave planar optical interconnections using highly multiplexed polymer waveguide holograms", *J. Lightwave Technology*, 10(7),1-10,(1992)
20. P.K. Kostuk, M. Kato, Y.T. Huang,"Polarization properties of substrate-mode holographic interconnects", *Applied Optics*, 29(26),3848-3854,(1990)
21. Z. Fu, C. Zhou, R.T. Chen, "Waveguide-hologram-based wavelength-multiplexed pseudoanalog true-time-delay module for wideband phased-array antennas", *Applied Optics*, 38(14) ,3053-3059,(1999)
22. G. Kim, R.T. Chen, "Three-dimensionally interconnected multi-busline bidirectional optical backplane", *Optical Enginnering*, 38(9), 1560-1566,(1999)
23. X. Deng, D. An, F. Zhao, R. T. Chen, V. Villavicencio, "Temperature sensitivity of passive holographic wavelength division multiplexers/demultiplexers",(submitted to *Applied Optics*)
24. X. Deng, F. Zhao, R. Chen, "Optimal design of volume holographic wavelength division multiplexers /demultiplexers", *Proc. SPIE* , (this issue)
25. L. Li, "Multilayer modal method for diffraction gratings of arbitrary profile, depth, and permittivity", *J. Opt. Soc. Am.*, A10(12),2581-2591,(1993)
26. L. Li, "Formulation and comparison of two recursive matrix algorithms for modeling layered diffraction gratings", *J. Opt. Soc. Am.* , A13(5),1024-1035,(1996)
27. M.G. Moharam,E.B. Grann, D.A. Pommet, T.K. Gayload, "Formulation for stable and efficient implementation of the rigorous coupled-wave analysis of binary gratings", *J. Opt. Soc. Am.*, A12(5),1068-1076,(1995)
28. M.G. Moharam, D.A. Pommet, E.B. Grann, T.K. Gayload, "Stable implementation of the rigorous coupled-wave analysis for surface-relief gratings:enhanced transmittance matrix approach", *J. Opt. Soc. Am.*, A12(5), 1077-1086, (1995)
29. R.R. A. Syms, *Practical Volume Holography*, Clarendon Press (Oxford,1990)
30. H. Ishio, J. Minowa, K. Nosu,"Review and status of wavelength-division-multiplexing technology and its application", *J. Lightwave Technology*, LT-2(4),448-463,(1984)
31. Y. Ishii, T. Kubota, "Wavelength demultiplexing in multimode fiber that uses optimized holographic optical elements", *Applied Optics*, 32(23),4415-4422,(1993)
32. T. Blesik, private communications (August 17,1999).
33. W.J. Gambogi, A.M. Weber, and T.J. Trout, "Advances and applications of DuPont holographic photopolymers", *SPIE*, Vol. 2043,2-13,(1993)
34. W.J. Gambogi, W.A. Gerstadt, S.R. Mackara, A.W. Weber, "Holographic transmission elements using improved photopolymer films", *Proc. SPIE*, Vol. 1555,256-267,(1991)
35. W.J. Gambogi, K. Steijin, S. Mackara, T. Duzick, B. Hamzavy, J. Kelly, "HOE imaging in DuPont holographic photopolymers", *SPIE*, Vol. 2152,282-293,(1994)
36. C. Zhao, J. Liu, Z. Fu, R.T. Chen,"Shrinkage-corrected volume holograms based on photopolymeric phase media for surface-normal optical interconnects", *Appl. Phys. Lett.*, 71(11),1464-1466,(1997)
37. J.-H. Yeh, R.K. Kostuk, "Substrate-mode holograms used in optical interconnects: design issues", *Applied Optics*, 34(17),3152-3164,(1995)
38. J.-H. Yeh, R.K. Kostuk, "Design issues for substrate mode holograms used in optical interconnects", *Proc. SPIE*, Vol. 2176,207-217,(1994)